Local distortions revealed by neutron holography in $SnCd_{0.0026}$ alloy

Alex Szakál,* Márton Markó,† and László Cser‡
Wigner Research Centre for Physics, Konkoly Thege M. út 29-33, H-1121 Budapest, Hungary
(Received 11 January 2016; revised manuscript received 20 April 2016; published 24 May 2016)

Local distortions of the ideal periodic structure in crystals around impurity atoms play an important role in various physical properties of materials. The aim of this study was to investigate the static distortions around cadmium impurity atoms in a $SnCd_{0.0026}$ single crystal using atomic resolution neutron holography technique. The cadmium nucleus was used as an inside detector to measure the holographic interference pattern from which the three-dimensional (3D) atomic arrangement of tin nuclei around the cadmium impurities was reconstructed. Detailed analysis of the reconstructed image revealed the 3D static displacements of Sn atoms around the impurity. It was found that the crystal structure contracts around the cadmium impurity atom and the displacements tend to transform the crystal to the α phase. The local contraction of the lattice was used to explain the slower phase transformation to α-Sn phase when Cd impurity atoms are present. The study shows the ability of neutron holography to measure 3D displacements around impurities which can be used, e.g., to understand the mechanisms that block the phase transformations in the presence of impurities.

DOI: 10.1103/PhysRevB.93.174115

I. INTRODUCTION

Measurement of local distortions caused by impurity atoms is important for understanding of various physical processes (e.g., effect on phase transformations, impurity hardening). Little is known about the details of the microscopic deformations caused by impurity atoms, but recent developments in experimental methods allow us to measure the local structure of crystalline materials around specific atoms and reveal the deviations from the ideal periodic lattice in a direct way. The most widely used techniques for direct 3D visualization of the local structure are x-ray fluorescence holography (XFH) [1–3], neutron holography (NH) [4–6], and photoelectron holography (PH) [7,8]. Up to now little is known about how the impurity atoms deform the host lattice and change the macroscopic properties of the host material.

The well established diffraction techniques probe mainly the long-range order and few methods can give direct or even indirect information about the local structures. The most widespread direct method is x-ray absorption fine structure (XAFS) [9] which measures only the radially averaged structure and is—due to physical limitations—very nearsighted. The most well known indirect methods are diffuse scattering and reverse Monte Carlo (RMC) [10] methods. RMC fits data of different types (x-ray/neutron diffraction, EXAFS, anomalous x-ray scattering) by tuning a model of atoms in a volume and analyzing the model which fits best to the measured data. The analysis of static diffuse scattering is done by either fitting analytically calculated model functions or by using Monte Carlo methods [11]. Contrary to that, atomic resolution holography (ARH) with x rays and neutrons provides a direct three-dimensional picture of the crystal lattice around a selected type of atom up to few nanometer distance. Although holographic experiments were made on numerous different samples, recent studies are mainly focused on the intensity variations caused by the lattice vibrations [12–14]. Radial displacements around impurity atoms were analyzed in a few studies [15,16], but to our knowledge tangential displacements were not detected. The aim of the present research was to analyze the neutron hologram measured on the tetragonal allotrope of tin where besides radial displacements tangential ones around cadmium impurities were expected due to the lower symmetry of the crystal structure compared to the previous samples used for holographic experiments.

II. EXPERIMENT

The experiment was performed on a Sn single crystal alloyed with Cd impurity atoms. The diameter of the spherically shaped crystal was 7 mm. The cadmium content was measured using the PGAA instrument [17] at the Budapest Neutron Centre, proving the presence of 0.26 at. % cadmium in the sample. Neutron diffraction experiments at the D9 diffractometer at ILL showed that the crystal structure remained in the β-Sn phase with bct crystal structure. The lattice constants of β-Sn are $a = 5.8318$ Å and $c = 3.1819$ Å [18]. The orientation of the crystal was measured enabling us to use the symmetry operations on the reconstructed image improving image quality. It was shown by neutron holography [19] earlier, that cadmium occupies the substitutional position in the tetragonal tin lattice.

The cadmium atom is used as a detector in the sample, and the position of the neighboring atoms can be investigated by the neutron holographic experiment (i.e., internal detector holography). The cadmium crystallize in the hcp structure with $a = 2.97887$ Å and $c = 5.61765$ Å [20]. This structure is very different from the crystal structure of β-Sn explaining the low solubility of cadmium in tin [21]. The difference between the crystal structures and the low solubility intimate big distortions of the host lattice around the cadmium impurity. Thus, $SnCd_{0.0026}$ can be considered as an ideal model system for the measurement of the local 3D distortions.

The holography measurement was done at the Budapest Research Reactor in the thermal triple-axis and neutron holographic spectrometer. The details of the instrument and

*szakal.alex@wigner.mta.hu
†marko.marton@wigner.mta.hu
‡cser.laszlo@wigner.mta.hu

the first reconstruction of the hologram was reported in [19]. In the following a short summary of the most important details and additional information about the data processing are given. Thermal neutrons with 1.00 Å wavelength were used in the experiment to excite the ^{113}Cd isotopes of Cd nuclei embedded in the sample. The prompt-γ yield was measured by a BGO scintillation detector capable of measuring the prompt-γ photons emitted by the cadmium nucleus with sufficiently high count rate, efficiency, and relaxed energy resolution. The γ detector was equipped with a thick sandwich shielding to filter out the high γ background of the reactor environment. On the outside of the shielding, 15 cm borated paraffin with cadmium sheets was used to capture the neutron background and a 20-cm-thick lead box filtered the γ photons. Shielding against neutrons was important because the neutrons reaching the detector can activate the stainless steel house of the γ detector. The entrance hole of the detector shielding was covered with plastic containing ^{6}Li to filter the diffracted neutrons from the sample. ^{6}Li was used at this place because the neutron capture is not followed by emission of γ photons. The measured photons were filtered by a discriminator window set to the energy of the prompt-γ photon of cadmium. The sample-detector distance was 15 cm. The plane of the χ circle of the Eulerian cradle was aligned parallel to the incoming beam to measure the inside detector hologram.

The holographic interference pattern was measured by mapping the γ intensity by changing the χ and ϕ angles of the Eulerian cradle and keeping the position of the γ detector fixed. The χ angle was scanned between -60° and 60° with steps of 2° and the ϕ angle between 0° and 360° with the same step size. The measured intensity map is shown in Fig. 1(a). During the 15 days of measurement 1.5×10^9 counts were measured. The raw interference pattern was corrected for the slow variation of reactor power by using a low efficiency monitor detector and dividing the γ intensity by the counts of a monitor detector. It is a remarkable advantage of inside detector holography that neither Bragg peaks nor diffuse scattering can be seen on the interference pattern because the detector measured the γ photons emitted by cadmium atoms instead of the scattered neutrons by the sample. The most challenging part of the data reduction process is the baseline determination. The hologram has an inherently high but constant baseline due to the reference wave, but imperfections in centering the sample in the beam make the background slowly varying, as seen in Fig. 1(a). This slow background variation can be corrected by the application of high pass Fourier filtering. The parameters of filtering have to be chosen carefully. On one side, if less Fourier components are discarded the spurious intensity can hide the hologram which can be checked by looking at the flatness of the filtered interference pattern. On the other hand, if too much Fourier components are discarded then serious distortions appear on the reconstructed image. This situation can be excluded by the reconstruction of a filtered model hologram. The model of the measured hologram was constructed taking into account the atoms inside a sphere with radius of 10 Å around the impurity Cd atom. The result of the model calculations was that filtering in χ direction is not possible because the removal of even the first Fourier component severely distorts the hologram. The optimal filtering was found to be the removal of the first four Fourier components row by row in ϕ direction which eliminated the slow variation dominating Fig. 1(a) but do not cause distortions on the reconstructed model hologram. The interference pattern after baseline subtraction is shown in Fig. 1(b). It is important to note that however the holographic interference pattern in Fig. 1(b) is covered by the statistical noise in the individual pixels, the real space image can be reconstructed because the signal to noise ratio (SNR) of the real space image depends on the total count number of the interference pattern instead of the counts registered in the individual pixels [22].

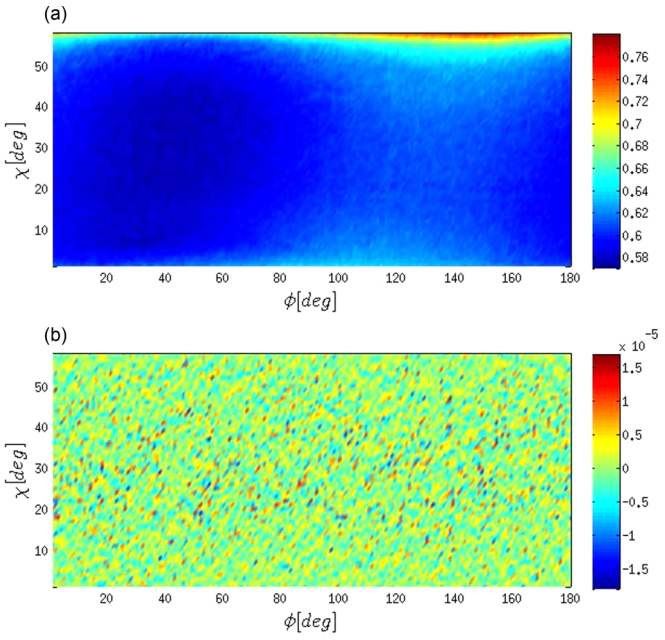

FIG. 1. The measured interference pattern in function of Euler angles χ and ϕ. (a) Counts normalized with the monitor detector. (b) Hologram after baseline subtraction.

The measured orientation of the sample allowed us to extend the measurement domain by using the symmetries of the crystal structure. The benefit of using symmetry operations is the decrease of noise on the reconstructed image [22]. However, the use of these symmetry operations could restrict the directions of measurable distortions, in the present case the single impurity atom cannot break the local symmetry and the local symmetries found around an atom of the host lattice will remain. The atomic arrangement around the Cd atom was reconstructed inside a cuboid using the Helmholtz-Kirchoff integral as proposed by Barton [23]. The edges of the cuboid was parallel to the axes of the elementary cell of the crystal. The reconstruction was done between -1 and 6.5 Å in the direction of **a** and **b** axis and from -0.5 to 4.3 Å in the direction of the **c** axis with a fine grid resolution of 0.025 Å.

III. RESULTS AND DISCUSSION

The image of neighboring atoms can be seen in the reconstructed image nearby the positions predicted by the crystal structure of pure β-Sn [19]. Thus, to study the distortions, peak centers and amplitudes had to be determined with higher accuracy. The maximal—or minimal in case of

TABLE I. Parameters extracted from the reconstructed image. $\Delta X, \Delta Y, \Delta Z$ are the coordinates of displacements of neighboring atoms from the undistorted β-Sn structure. The displacement in radial direction is calculated using the points with maximal amplitude (ΔR_{center}) and using the peak amplitudes and the cosine rule (ΔR_{amp}). The c/a ratio of the imaginary bct crystal assigned to each neighbor is also shown. P_{calc} is the estimated pressure needed for the observed radial distortions.

Neighbor	ΔX (Å)	ΔY (Å)	ΔZ (Å)	ΔR_{center} (Å)	ΔR_{amp} (Å)	Amp. (a.u.)	SNR [1]	$(\frac{c}{a})_{\text{calc}}$ (a.u.)	P_{calc} (GPa)
First	0	−0.141	−0.02	−0.138	−0.217	4.571	15.80	0.5589	33.1
Third	0	−0.545	0.289	−0.193	−0.15	−7.855	14.47	0.7523	22.5
Fourth	−0.166	−0.166	0.259	−0.113	−0.113	−7.739	4.44	0.6727	12.4
Fifth	0	−0.591	0.323	−0.043	−0.000	7.309	8.03	0.7399	0

negative peaks—amplitude was searched around the theoretical position in a region of interest. In addition to the images of the atoms, the reconstructed image contains spurious peaks due to the interference of side oscillations of atomic peaks, imperfection of background removal, and statistical noise. The signal to noise ratio (SNR) [22] was calculated for the neighboring shells and the values are shown in Table I. It was verified that the points with extremal amplitude belong to the atomic peaks and not to a side oscillation or other artifact. The first, third, fourth, and fifth neighbors were found using this algorithm, but the second neighbor was ruled out by the cosine rule [15]. The coordinates and amplitudes of the atomic peaks observed on the reconstructed image were recorded. Cuts of the reconstructed image in the planes where the amplitude of atomic peaks have extremal values are shown in Fig. 2.

The radial displacements and the 3D distortion field around the cadmium impurity can be studied in a direct way on the reconstructed hologram. In the following the radial displacements are discussed first and then the displacements in 3D are analyzed. The coordinates of the displacement vectors of peak centers, the amplitudes of them, and the radial displacements are summed up in Table I.

The radial displacements are plotted in Fig. 3. There are two methods available to measure the displacements in a radial direction on a single-energy hologram. The peak centers show the positions of neighboring atoms but at the same time the amplitudes can be used for the precise determination of radial distances [15] by utilizing the $\cos(kr)$ dependence of the amplitude on the radial distance r. In order to use the amplitudes for the determination of radial distances they must be normalized to a measured peak. The fourth neighbor was chosen for normalization because the slope of the $\cos(kr)$ function is the smallest there, thus any error in the position determination has less influence on the other radial distances. The results of the two determinations are shown in Table I and Fig. 3. The equivalence of the radial position measured by the two methods proves that the peaks correspond to atomic images because the distance dependence of amplitudes follow the cosine rule.

Besides the radial distance from the detector atom, the amplitude of the reconstructed peak is influenced by the amplitudes of the positional fluctuations around the equilibrium positions [2]. The displacement values measured by using the peak amplitudes and the peak centers do not differ significantly, i.e., meaning that the amplitudes of positional fluctuations are similar for all neighbors.

The radial displacements are contractive around the Cd impurity which was unexpected, as the atomic radius of a Cd atom is larger than the atomic radius of tin. In the case of metals the atomic radius is an insufficient measure of the size because the outer electrons become delocalized. In the case of alloys the atomic volume changes according to Zen's law [24]. This empirical law states that the mean atomic volume changes linearly with composition. The atomic volume of Cd is 13.1 cm^3/mol which is significantly smaller than the 16.3 cm^3/mol atomic volume of Sn explaining qualitatively the measured contraction of the Sn lattice.

As it is seen in Fig. 3, the radial displacements around the Cd impurity decrease within 5 Å distance. A computer model of the structure was built where the Cd atoms were distributed randomly on the sites of the Sn lattice. The distribution of the distance to the first Cd neighbor was calculated on the model system. In the case of 1.07% Cd concentration, i.e., at the solubility limit of Cd, the average value of the Cd-Cd distances was 12.02 Å with 4.27 Å standard deviation. Using the 0.27% Cd concentration of the sample used in the experiment the average Cd-Cd distance was 19.25 Å with 6.94 Å standard deviation. Based on the model and the measured displacement field, it can be concluded that the impurities can be considered independent from each other because the displacement fields only start to overlap when the Cd concentration reaches the phase boundary of solid solubility. By increasing the Cd content beyond the solubility limit the displacement fields do not overlap more but the formation of a Cd phase is started.

There are two sources of distortions around impurity atoms. The first is the different interatomic potentials between the host atoms and between the impurity atom and the host atoms [25]. The second source of distortions in the case of metals is the potential of charge oscillations of conduction electrons scattered on the impurity atom, i.e., the Friedel oscillations [26],

$$\Delta\rho = -\frac{1}{2\pi^2 R^2}\sum_L (2L+1)\sin(\eta_L) \times [\cos(2k_F R + \eta_L - L\pi) - \cos(\eta_L - L\pi)], \quad (1)$$

where $\Delta\rho$ is the variation in local charge density, R is the distance from the scatterer, k_F is the Fermi wave vector, and η_L is the phase shift. The phase shifts satisfy the Friedel sum rule

$$Z = \frac{2}{\pi}\sum (2L+1)\eta_L(k_F), \quad (2)$$

where Z is the impurity valency relative to the host lattice. The charge oscillations can be reasonably well described using the first two to three components in (1).

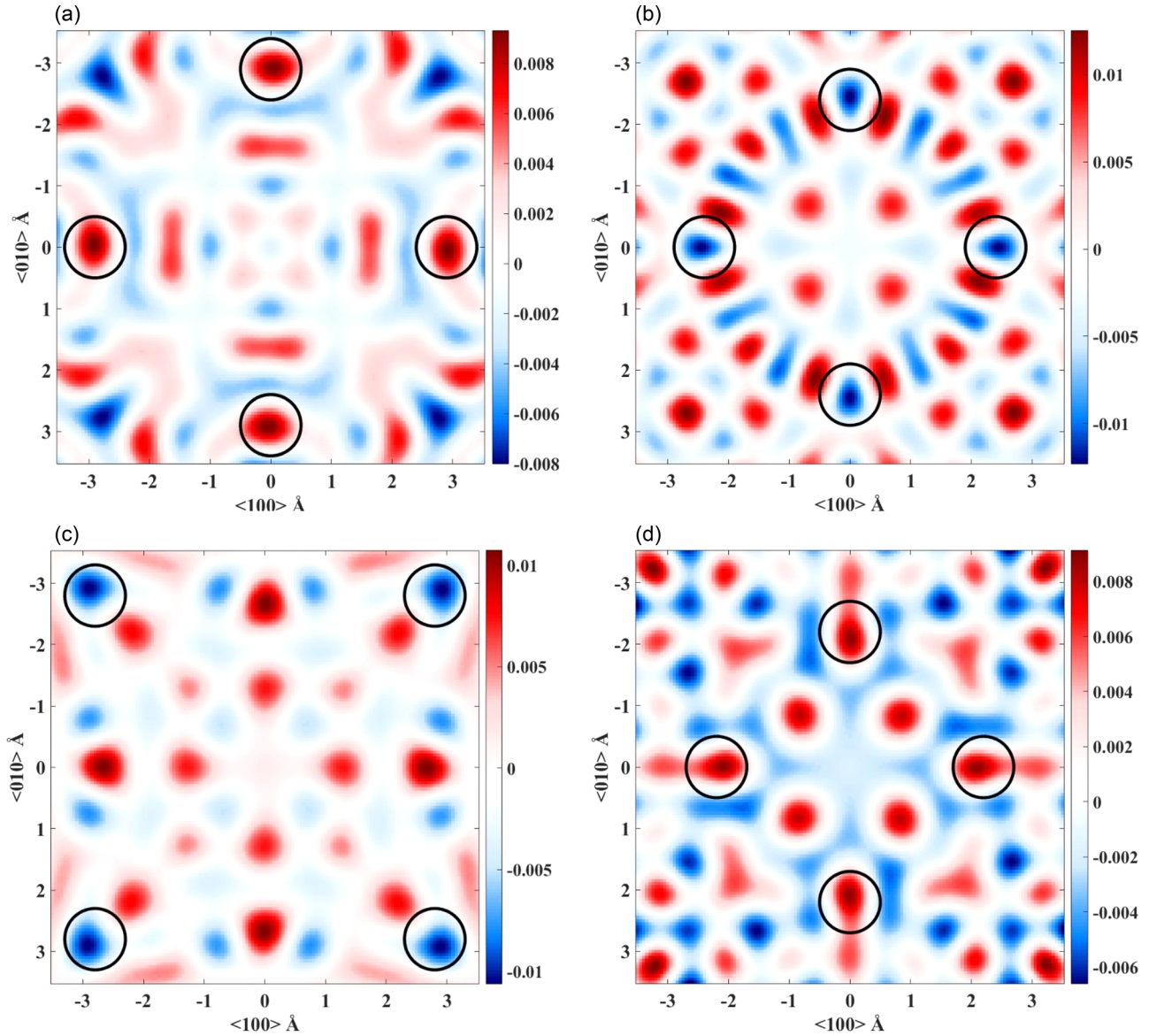

FIG. 2. The amplitude of the reconstructed hologram on planes perpendicular to the [00z] direction. The location of the atomic peaks are marked by black circles. (a) Plane of first neighbors at $z = 0.775$ Å. (b) Plane of third neighbors at $z = 2.675$ Å. (c) Plane of fourth neighbors at $z = 1.85$ Å. (d) Plane of fifth neighbors at $z = 4.3$ Å.

It was found in a previous study on a dilute $PbCd_{0.026}$ system [15] that the measured radial displacements can be explained by using Friedel oscillations. However, for $SnCd_{0.0026}$ solely this model did not fit our data although we used a simulated annealing algorithm for fitting with Friedel components $L = 0,1,2$. The simulated annealing model was important in order to avoid local minima during the fitting process. It was impossible to get a satisfactory fit even though the model had three free parameters: the scaling constant and two independent phase shifts, indicating that solely the Friedel oscillations cannot explain the distortions.

Thus, the effect of the different interatomic potential has to be included in the model besides the Friedel oscillations. The distortions caused by the different interatomic potentials decrease with R^{-2} when the concentration of impurities is low [25], i.e., they do not interact with each other. This term was included in our model and the number of Friedel components was decreased to the minimal $L = 0,1$ leading to the fitting function

$$\Delta R = C_{\text{Friedel}} \Delta\rho_{L=0,1} + C_{\text{pot}}/r^2, \tag{3}$$

where ΔR is the radial displacement, $\Delta\rho_{L=0,1}$ is the charge oscillation, and C_{Friedel} and C_{pot} are scaling constants. The function was fitted to the average of the radial displacements determined by the peak centers and the amplitudes. The fitted curve is presented in Fig. 3, showing additionally the separated contribution of the interatomic potential and the Friedel oscillation. It is seen that the interatomic potential plays the major role and dominates over the effect of Friedel oscillations.

The atomic positions were determined using the coordinates of centers of atomic peaks which allow us to study the displacements not just radially but in 3D around the impurity atom. Contrary to the previously investigated systems, nonradial displacements of atoms are allowed due to the lower symmetry

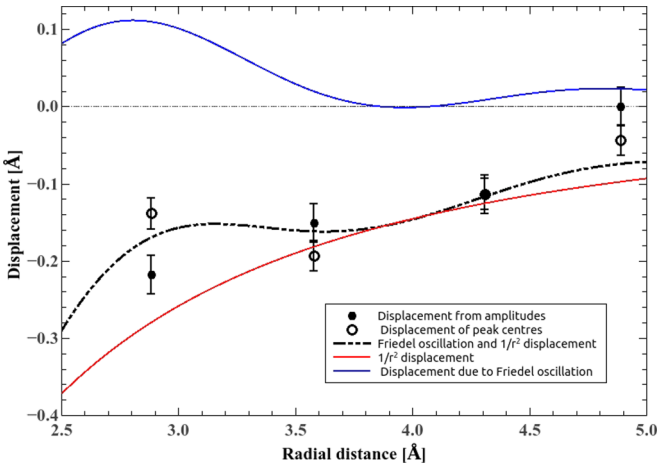

FIG. 3. Radial displacements of the atoms around the cadmium impurity. Filled circles show the displacements calculated from the amplitude of the image, empty circles show the positions of the peak centers. Dashed line represents the fitted curve to the displacements, the red line is the contribution of the C_{pot}/r^2 displacement field and the blue line is the contribution of the Friedel oscillations. The fitted parameters: $C_{\text{Friedel}} = 24.48 \pm 12$, $\eta_1 = 71.59 \pm 0.4$, $C_{\text{pot}} = -2.3 \pm 0.8$.

of tetragonal Sn compared to the previously investigated cubic systems. The numerical values of the displacements are given in Table I and a scheme of the displacements is shown in Fig. 4.

This interpretation of the 3D reconstruction of displacements leads to the idea of comparing the local structure around the impurity atom to the structure in the closely related α-Sn phase. There is a phase transition of β-Sn to an allotropic form called α-Sn or gray tin with diamond structure. The phase transformation occurs at 13.2 °C and also known as "tin pest." This phase transformation has technological importance because the material breaks up and loses integrity. The crystal structure of β-Sn can be transformed into a diamond lattice if the c/a ratio is increased from 0.546 of β-Sn to $\sqrt{2}$ of the diamond lattice. A c/a ratio can be defined for every Sn neighbor of the Cd impurity in the following way. The Sn neighbors seen in the hologram have nonzero coordinates parallel to the c and a axis of the crystal, thus the distorted positions define the a and c lattice constants of a distorted bct lattice for each neighbor. The distorted c/a ratio shown in Table I for the neighbors seen in the reconstructed hologram is increased significantly for all neighbors except the first neighbor where it increased only slightly. The increase of c/a ratio shows the tendency of the structure to transform towards the diamond lattice which is the stable phase at lower temperature.

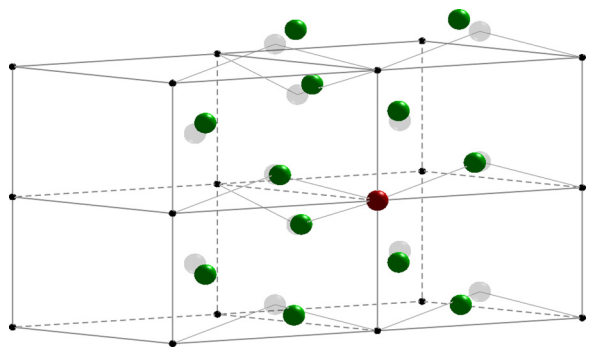

FIG. 4. Representation of the displacement field of the neighboring Sn nuclei around the Cd impurity. The red sphere marks the position of the Cd impurity nucleus. Transparent gray spheres show the positions of the Sn nuclei in the undistorted crystal, while green spheres are placed at the measured positions.

The phase transformation of β-Sn to α-Sn can be blocked by applying compressive stress, i.e., pressure on the sample or equally by alloying with certain elements, e.g., bismuth of antimony. The addition of Cd to Sn also slows down the phase transformation [27]. It is supposed [28] that the local displacements and stresses around impurity atoms play an important role in this process, but to our knowledge, deeper explanation has not been given. Although the direction of lattice distortions points towards the diamond lattice, in order to form the α-Sn phase, the lattice should expand significantly. Contrary to that, our measurements reveal the contraction of the lattice around the impurity. The contraction of the lattice can be reached by compressive stress or equivalently by external pressure. The p-T phase diagram of Sn [29] shows that by increasing the pressure, the temperature of the phase transformation can be lowered, and by reaching a threshold, the transformation is stopped. Based on the this phenomenon we conclude that the *contraction* of the local lattice, i.e., the appearance of a compressive stress, can be the reason for the reduction of the speed of transformation to the α-Sn phase.

The magnitude of pressure—leading to similar distortions as the observed ones of the lattice—was estimated using the changes in radial distances of the neighbors. The estimation was done using Hooke's law and the different strains were calculated from the radial displacements. The isotropic modulus of elasticity of Sn was used for the calculation. The resulting pressures are shown in Table I. These pressures are comparable to the pressure at the phase boundary [29] which is 10 kbars at 50 K. The calculated pressures are higher than this boundary pressure, thus presumably a region around the cadmium where the transformation is blocked is present leading to slower phase transformation because the formation of nucleation centers becomes more difficult.

IV. CONCLUSION

In the present study neutron holography was used to measure the local distortions around Cd impurity atoms in a β-Sn single crystal. Although local structure measurement with atomic resolution holography techniques has been done in several studies, according to our knowledge it was not applied to measure the distortion field in 3D before, because the previously measured samples had cubic symmetry, thus only radial displacements were possible. Contrary to that, the studied β-Sn crystal has body centered tetragonal structure allowing nonradial displacements of atoms around the Cd impurity. The holographic measurement was performed at the dedicated instrument of the Budapst Research Reactor. The atomic arrangement was reconstructed from the holographic interference pattern and a precise determination of peak centers and amplitudes were carried out. First, the radial displacements were analyzed and it was shown that the crystal shrinks around the impurity atom.

The measured radial displacements can be explained by a model containing the distortions caused by the different interatomic potential and the Friedel oscillations. The fitted model shows that the main source of displacements is the different interatomic potential. Analysis of the 3D distortions cleared up that the distortions had significant tangential components. The distorted structure around the cadmium impurity points towards the closely related diamond lattice which is the stable phase of Sn below 13.2 °C. The $\beta \rightarrow \alpha$ phase transformation can be slowed down by the addition of a small amount of Cd to Sn. A phenomenological explanation was given for this observation by using the measured local distortions. It is known that macroscopic compressive stress blocks the phase transformation and our study shows that the cadmium impurity has a similar effect on the lattice locally as the macroscopic compressive strain, i.e., the lattice is shrinked.

These findings extend our knowledge about the underlying mechanism leading to blocking or slowing down the phase transformation by adding a possible explanation using the measured local distortions. This explanation supports the assumption reported in the literature that the local distortions and strains play a key role in slowing down the phase transformation. This study demonstrates the use of atomic resolution neutron holography for the understanding of how the macroscopic properties of a bulk material is changed by a small amount of impurity atoms. Although carrying out neutron holographic measurements is elaborate due to the low luminosity of current sources, the authors believe that almost routine experiments could be done at the European Spallation Source foreseen to be orders of magnitudes brighter than the current neutron sources.

ACKNOWLEDGMENT

The authors acknowledge the financial support of Project No. KMR-12-1-2012-0226 granted by the National Development Agency of Hungary.

[1] T. Gog, P. M. Len, G. Materlik, D. Bahr, C. S. Fadley, and C. Sanchez-Hanke, Phys. Rev. Lett. **76**, 3132 (1996).
[2] K. Hayashi, N. Happo, and S. Hosokawa, J. Electron Spectrosc. Relat. Phenom. **195**, 337 (2014).
[3] M. Tegze and G. Faigel, Nature (London) **380**, 49 (1996).
[4] B. Sur, R. B. Rogge, R. P. Hammond, V. N. P. Anghel, and J. Katsaras, Nature (London) **414**, 525 (2001).
[5] L. Cser, B. Faragó, G. Krexner, I. Sharkov, and G. Török, Phys. Rev. Lett. **89**, 175504 (2002).
[6] K. Hayashi, K. Ohoyama, S. Orimo, Y. Nakamori, H. Takahashi, and K. Shibata, Jpn. J. Appl. Phys. **47**, 2291 (2008).
[7] G. R. Harp, D. K. Saldin, and B. P. Tonner, Phys. Rev. Lett. **65**, 1012 (1990).
[8] H. Daimon, J. Surf. Sci. Nanotechnol. **10**, 169 (2012).
[9] D. E. Sayers, E. A. Stern, and F. W. Lytle, Phys. Rev. Lett. **27**, 1204 (1971).
[10] R. L. McGreevy and L. Pusztai, Mol. Simul. **1**, 359 (1988).
[11] T. R. Welberry and D. J. Goossens, Acta Crystallogr. Sect. A **64**, 23 (2008).
[12] S. Hosokawa, N. Happo, and K. Hayashi, Phys. Rev. B **80**, 134123 (2009).
[13] W. Hu, K. Hayashi, T. Yamamoto, N. Happo, S. Hosokawa, T. Terai, T. Fukuda, T. Kakeshita, H. Xie, T. Xiao, and M. Suzuki, Phys. Rev. B **80**, 060202 (2009).
[14] S. Hosokawa, N. Happo, T. Ozaki, H. Ikemoto, T. Shishido, and K. Hayashi, Phys. Rev. B **87**, 094104 (2013).
[15] L. Cser, G. Krexner, M. Markó, I. Sharkov, and G. Török, Phys. Rev. Lett. **97**, 255501 (2006).
[16] W. Hu, K. Hayashi, K. Ohwada, J. Chen, N. Happo, S. Hosokawa, M. Takahasi, A. A. Bokov, and Z.-G. Ye, Phys. Rev. B **89**, 140103 (2014).
[17] Z. Révay, T. Belgya, Z. Kasztovszky, and J. Weil, Nucl. Instrum. Methods Phys. Res. Sect. B **213**, 385 (2004), 5th Topical Meeting on Industrial Radiation and Radioisotope Measurement Applications .
[18] V. T. Deshpande and D. B. Sirdeshmukh, Acta Crystallogr. **14**, 355 (1961).
[19] M. Markó, A. Szakál, G. Török, and L. Cser, Rev. Sci. Instrum. **81**, 105110 (2010).
[20] R. Wyckoff, *Crystal Structures*, No. 1 (Wiley, New York, 1963).
[21] H. W. Rayson, C. W. Goulding, and G. V. Raynor, Metallurgia **59**, 57 (1959).
[22] M. Markó, L. Cser, G. Krexner, and G. Török, Meas. Sci. Technol. **20**, 015502 (2009).
[23] J. J. Barton, Phys. Rev. Lett. **67**, 3106 (1991).
[24] E-an Zen, Am. Metal. **41**, 523 (1956).
[25] M. A. Krivoglaz, *Theory of X-Ray and Thermal-Neutron Scattering by Real Crystals* (Plenum, New York, 1969), Chap. II.
[26] G. BAUER, in *Neutron Scattering*, edited by G. Kostorz , Vol. 15, (Elsevier, Amsterdam, 1979), pp. 291–336.
[27] G. Tammann and K. L. Dreyer, Z. Anorg. Allgemeine Chem. **199**, 97 (1931).
[28] K. Puttlitz and K. Stalter, *Handbook of Lead-Free Solder Technology for Microelectronic Assemblies*, Mechanical Engineering (CRC, Boca Raton, FL, 2004), Chap. 22.4.C.
[29] J. F. Cannon, J. Phys. Chem. Ref. Data **3**, 781 (1974).